

First-Order Antiferromagnetic Transition and Novel Gapless Excitation in a 4f Zigzag Chain Compound YbCuS₂

Fumiya Hori¹, Katsuki Kinjo¹, Shunksaku Kitagawa¹, Kenji Ishida¹, Yudai Ohmagari², and Takahiro Onimaru²
¹*Department of Physics, Kyoto University, Kyoto 606-8502, Japan*

²*Department of Quantum Matter, Graduate School of Advanced Science and Engineering, Hiroshima University, Higashihiroshima 739-8530, Japan*

We report on the ^{63/65}Cu–nuclear magnetic resonance and nuclear quadrupole resonance (NQR) studies of trivalent Yb zigzag chain compound YbCuS₂. Sharp NQR signals were observed in the paramagnetic (PM) state. Below $T_O \sim 0.95$ K, the multi peaks induced by the internal magnetic fields arising from the antiferromagnetic (AFM) ordered moments appear and coexist with the PM signal down to 0.85 K, evidencing the first-order AFM phase transition at T_O . In addition, the nuclear spin-lattice relaxation rate $1/T_1$ abruptly decreases below T_O and shows the T -linear behavior below 0.5 K. The significant large $1/T_1T$ value ($1/T_1T = 14 \text{ s}^{-1} \text{ K}^{-1}$) strongly suggests the presence of the novel gapless spin excitation in low temperature region.

Frustration effects in low-dimensional quantum spin systems lead to the suppression of long-range order and non-trivial ground states [1]. A typical example of such a frustrated quantum spin system is the $S = 1/2$ zigzag-chain with competition between the nearest-neighbor and next-nearest neighbor exchange interaction [2, 3]. In this system, a variety of non-trivial quantum phenomena such as spin dimerization, a $1/3$ -magnetization plateau, and vector chirality have been theoretically suggested [4–6] and experimentally confirmed in $(\text{N}_2\text{H}_5)\text{CuCl}_3$, $\text{Rb}_2\text{Cu}_2\text{Mo}_3\text{O}_{12}$, and so on [7–10].

Recently, frustrated spin systems formed by rare-earth elements have been intensively studied. The strong spin-orbit coupling and crystalline electric field (CEF) associated with 4f electrons of rare-earth ions such as Ce^{3+} and Yb^{3+} lead to highly anisotropic exchange interactions, providing a novel platform for the spin system. Many rare-earth-based frustrated compounds with kagomé, triangular, or honeycomb lattices have been studied. For example, YbMgGaO_4 [11–13] and NaYbSe_2 [14] with a triangular structure exhibit an unusual ground state due to the frustration. However, few rare-earth based compounds with a zigzag-chain structure have been found thus far.

YbCuS₂ is one such Yb-based zigzag-chain system. Figure 1(a) shows the crystal structure of YbCuS₂, which has an orthorhombic structure with the space group $P2_12_12_1$ (No. 19, D_2^4), where Yb atoms form the zigzag chains along the a -axis [15]. The electrical resistivity of YbCuS₂ has been reported to have semiconducting behavior with an activation energy of 0.08 - 0.28 eV [16]. From the Curie-Weiss behavior of the magnetic susceptibility $\chi(T)$, the effective magnetic moment μ_{eff} was estimated to be $4.62 \mu_B$, which is close to the value of the free Yb^{3+} ion ($4.54 \mu_B$). In general, the CEF level is important for understanding high-temperature and high-field magnetic response in rare-earth systems. However, the low-temperature properties are governed by only the CEF ground state which was reported to be an isolated Kramers doublet [17, 18]. The negative Weiss tempera-

ture $\theta_p = -31.6$ K with considering the CEF effect indicates the antiferromagnetic (AFM) interaction between the Yb magnetic moments. The magnetic specific heat divided by the temperature C_m/T shows a sharp peak at $T_O \sim 0.95$ K, suggesting a first-order (FO) phase transition. Since the transition temperature T_O is much lower than θ_p , YbCuS₂ is expected to be a frustrated spin system. Below 20 K, the magnetic entropy decreased from $R\ln 2$ expected for the Kramers doublet ground state. Here, R is the gas constant. The value of the magnetic entropy was only 20% of $R\ln 2$ at T_O , suggesting that the phase transition is suppressed by the fluctuation effect.

In addition, the unusual magnetic field H dependence of T_O was reported [18]. T_O is independent of H up to 4 T and has a maximum at approximately 7 T, and there are three anomalies in the H -swept AC susceptibility measured at low temperatures up to 18 T. These results suggest that a nontrivial ground state is realized in YbCuS₂.

To investigate the physical properties, particularly the origin of the T_O transition, from a microscopic point of view, we performed ^{63/65}Cu-nuclear magnetic resonance (NMR) and nuclear quadrupole resonance (NQR) measurements on polycrystalline samples of YbCuS₂. Our NQR results indicate that the FO AFM transition occurs at T_O . Moreover, the nuclear spin-lattice relaxation rate $1/T_1$ of ⁶³Cu at zero field abruptly decreases below T_O and exhibits T -linear behavior below 0.5 K, suggesting the presence of novel gapless fermionic excitations.

Polycrystalline samples of YbCuS₂ were synthesized by the melt-growth method [17, 18]. The polycrystalline samples were coarsely powdered to increase the surface area for better thermal contact. The powdered sample was mixed with GE 7031 varnish and solidified at zero magnetic field to avoid the preferential orientation of crystals in the NMR measurements and contact between crystals in the NQR measurements. A conventional spin-echo technique was used for the NMR and NQR measurements. A ³He-⁴He dilution refrigerator was used for the NQR measurements down to 0.075 K. ^{63/65}Cu-NMR spectra (with nuclear gyromagnetic ratios of $^{63}\gamma/2\pi =$

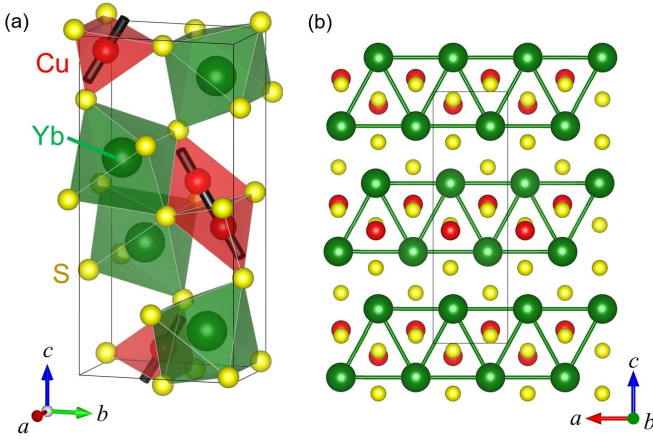


FIG. 1. (Color online) (a) Crystal structure of YbCuS_2 with the space group $P2_12_12_1$: the black sticks represent the principal axis of the electric field gradient tensor determined by calculation using the WIEN2k package.[19] (b) View from the b -axis: zigzag chains along the a -axis are formed by Yb atoms. The black box represents the unit cell. The structural image was produced using the VESTA program [20].

11.289 MHz/T and $^{65}\gamma/2\pi = 12.093$ MHz/T, respectively, and both with nuclear spin $I = 3/2$ were obtained as a function of H at the frequency $f = 19.5$ MHz. The principal axis of the electric field gradient (EFG) at the Cu site was determined by WIEN2k calculation using the density functional theory [19] since the principal axis was not determined experimentally due to a lack of a single crystal sample. The principal axis is represented by the black sticks in Fig. 1(a). $^{63/65}\text{Cu}-1/T_1$ was measured in YbCuS_2 and a reference compound LuCuS_2 to estimate the lattice contribution. $1/T_1$ was evaluated by fitting the relaxation curve of the nuclear magnetization after the saturation to a theoretical function for the nuclear spin $I = 3/2$. $1/T_1$ can be determined by a single relaxation component down to T_0 . However, the whole of the relaxation curve cannot be fitted to the single relaxation component below T_0 . Thus, we picked up the slowest components as shown in the supplemental material.

Figure 2(a) shows the H -swept $^{63/65}\text{Cu}$ -NMR spectrum measured at 4.2 K on the powdered sample. The quadrupole parameters ν_{zz} and η , which are explained subsequently, can be estimated by fitting the H -swept NMR spectrum to the simulated theoretical spectrum. In general, the total effective NMR Hamiltonian of a nucleus in H is given by

$$\mathcal{H} = \mathcal{H}_Z + \mathcal{H}_Q = -\frac{\gamma}{2\pi} h(1 + K)\mathbf{I} \cdot \mathbf{H} + \frac{h\nu_{zz}}{6} \left\{ (3I_z^2 - I^2) + \frac{1}{2}\eta(I_+^2 + I_-^2) \right\}, \quad (1)$$

where K is the Knight shift, h is the Planck constant, and I_{\pm} are the ladder operators of the nuclear spin I , which are defined as $I_{\pm} = I_x \pm iI_y$. $\nu_{zz} (\propto V_{zz})$ is defined as

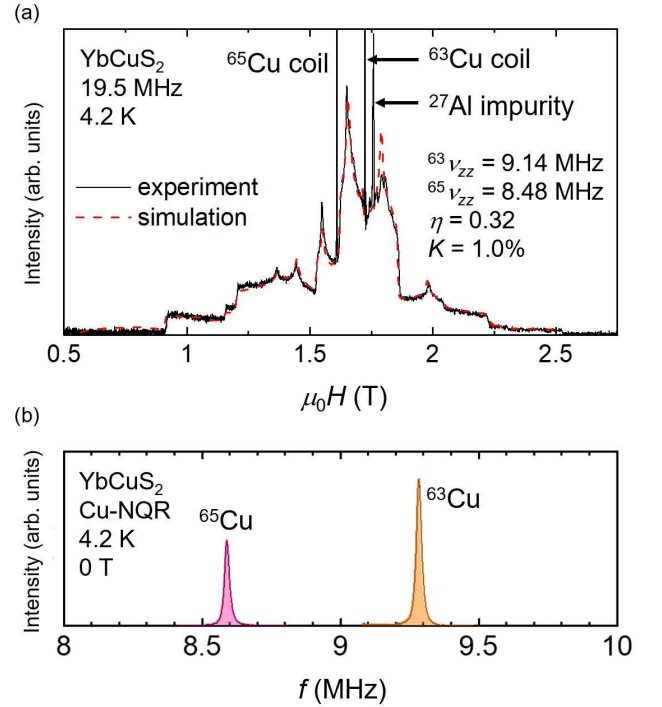


FIG. 2. (Color online) (a) NMR spectrum obtained by the field-swept method at a fixed frequency of 19.5 MHz and 4.2 K: the black solid and (red) dashed curves are the experimental result and the simulation of the NMR spectrum, respectively (see text). The three narrow lines in the NMR spectrum are signals from the Cu coil used for the NMR measurements and Al as an impurity arising from the NMR probe. (b) $^{63/65}\text{Cu}$ -NQR spectrum obtained by the frequency-swept method at 4.2 K.

$\nu_{zz} \equiv 3eV_{zz}Q/2I(2I - 1)$ with the electric quadrupole moment Q . η is an asymmetry parameter of the EFG defined as $\eta \equiv (V_{xx} - V_{yy})/V_{zz}$, where V_{ii} is the second derivative of the electric potential V ($V_{ii} = \partial^2 V / \partial x_i^2$). Since the NMR signal of each grain depends on the angle between the principal axis of the EFG in each grain and the direction of the magnetic field, the sum of the NMR signals for all solid angles could be observed in the non-oriented powder samples. The NMR spectrum was well fitted by the simulation with $K = 1.0\%$, $^{63}\nu_{zz} = 9.14$ MHz, $^{65}\nu_{zz} = 8.48$ MHz, and $\eta = 0.32$, as shown by the dashed line in Fig. 2(a).

We observed sharp $^{63/65}\text{Cu}$ -NQR signals at $^{63}\nu_Q = 9.28$ MHz and $^{65}\nu_Q = 8.59$ MHz, as shown in Fig. 2(b). The spectra were obtained by the frequency-swept method at 4.2 K without an external field. The obtained $^{63/65}\text{Cu}$ -NQR frequencies ν_Q at 4.2 K were consistently reproduced by $\nu_Q = \nu_{zz}\sqrt{1 + \eta^2/3}$ with the quadrupole parameters obtained above.

The occurrence of the FO AFM transition at T_0 was concluded from the following NQR results. Figure 3(a) shows the frequency-swept $^{63/65}\text{Cu}$ -NQR spectra measured at 4.2 K (upper panel) and 0.075 K (lower panel). Each paramagnetic (PM) peak splits into 6 peaks at

0.075 K [(A1) - (A6) for ^{63}Cu and (B1) - (B6) for ^{65}Cu]. The ^{63}Cu signals for (A1) and (A2) overlap with the ^{65}Cu signals for (B5) and (B6), respectively. As shown in Fig. 3(a), the observed ^{65}Cu peaks almost coincides with the ^{63}Cu signals scaled by the isotope ratio of the nuclear gyromagnetic ratio $^{65}\gamma/^{63}\gamma = 1.07$, not by that of the quadrupole moment $^{65}Q/^{63}Q = 0.93$. In addition, since the first moments of the NQR spectrum does not change across T_O , the EFG parameters are unchanged below T_O . Therefore, the NQR signals are split due to the appearance of internal magnetic fields at the Cu site rather than to the change of electric factors such as charge density wave, charge-ordered, or structural transitions.

We performed spectrum simulations to estimate the magnitude of the internal magnetic fields and their orientation with respect to the principal axis of the EFG at 0.075 K. As shown in the inset of Fig. 3(b), the 8 clearly visible peaks (A2) - (A5) and (B2) - (B5) can be fitted by the simulation with $\mu_0 H_{\text{int}} = 0.021$ T, $\theta = 77$ deg, and $\phi = 0$ deg, where $\mu_0 H_{\text{int}}$ is the absolute value of the internal fields, θ is the polar angle, and ϕ is the azimuthal angle of the internal fields from the principal axis of the EFG. The small internal field at the Cu site suggests the tiny Yb ordered moment [21]. However, the peaks (A1), (A6), (B1) and (B6) cannot be fitted by above parameters: these peaks can be reproduced by assuming a slightly larger internal field. Moreover, the presence of non-zero intensity between the peaks indicates the distribution of the internal fields. The wide distribution of the internal fields suggests an incommensurate or spiral magnetic structure, but a realized magnetic structure cannot be determined from the present measurement. Thus, elastic neutron scattering measurements are necessary, which will be performed in the near future.

The inset of Fig. 3(a) shows the temperature variations in the NQR spectra below 1.0 K. Multi-peaks appear below $T_O \sim 0.95$ K and coexist with the PM peak of $\nu_Q = 9.28$ MHz. The PM peak is not visible below 0.85 K. As shown in the main figure of Fig. 3(b), the internal field evaluated with the above simulation of the NQR spectra increases discontinuously below T_O , and the critical exponent β derived by fitting the relation $H_{\text{int}}(T) = H_{\text{int}}(0)[(T_O - T)/T_O]^\beta$ is 0.05, which is substantially smaller than the conventional mean-field value (0.5). These results indicate that the AFM transition is an FO phase transition, which is consistent with the sharp peak at T_O in the specific heat [18]. The FO AFM transition is unusual and has been observed when the AFM transition and structural transition occur simultaneously [22, 23]. In YbCuS_2 , since the NQR parameters are unchanged below T_O , a structural transition is unlikely. Therefore, the FO AFM transition is likely to be related to the magnetic frustration. In fact, a frustrated magnet EuPtSi shows a fluctuation-induced FO AFM transition without a structural phase transition [24, 25]. The magnetic properties of YbCuS_2 deserves further investigation.

Figure 4 shows the temperature dependence of the nu-

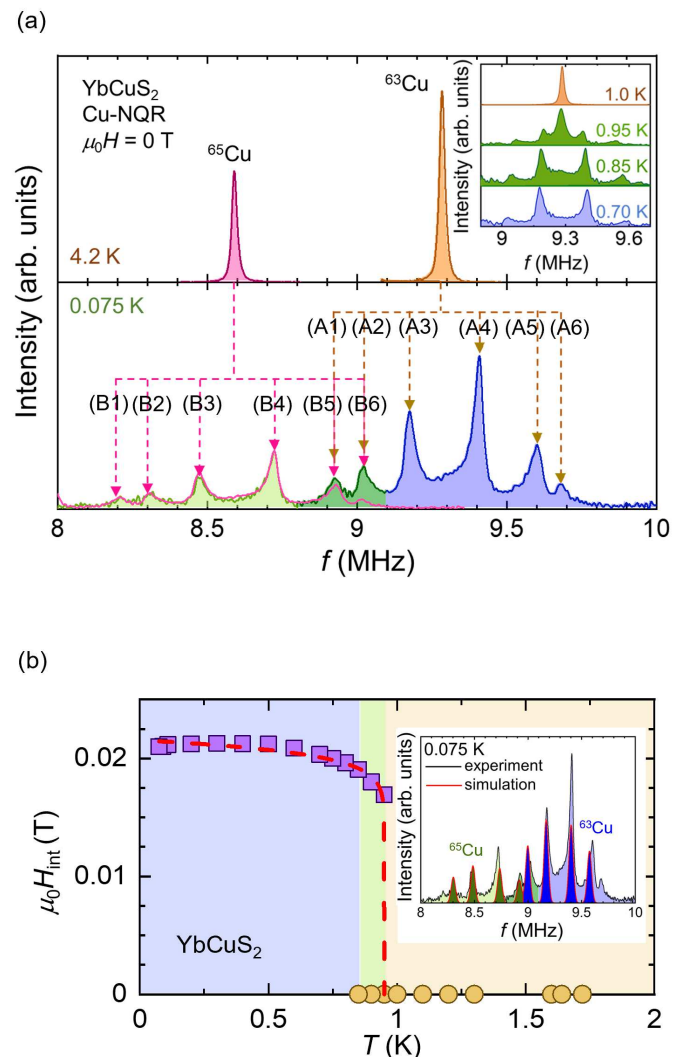


FIG. 3. (Color online) (a) $^{63}/^{65}\text{Cu}$ -NQR spectra obtained by the frequency-swept method at 4.2 K and 0.075 K: the pink curve represents the ^{63}Cu signals scaled by $^{65}\gamma/^{63}\gamma$ and shifted to the observed ^{65}Cu signals, which is expected ^{65}Cu signals with the appearance of internal fields. The inset shows the temperature variations of the ^{63}Cu -NQR spectrum for $0.7 \leq T \leq 1.0$ K. (b) Temperature dependence of the internal fields H_{int} estimated by simulation of the NQR spectra: the (red) dashed line represents the relation $H_{\text{int}}(T) = H_{\text{int}}(0)[(T_O - T)/T_O]^\beta$ with $\beta = 0.05$. The inset shows the frequency-swept $^{63}/^{65}\text{Cu}$ -NQR spectrum at 0.075 K, and the red solid curve is the simulation of the NQR spectrum.

clear spin-lattice relaxation rate $1/T_1$ measured at the ^{63}Cu signal of YbCuS_2 . Below T_O , $1/T_1$ was measured at the two peaks shown in the inset. To investigate contributions other than the $4f$ electrons, we also measured $1/T_1$ of a nonmagnetic reference compound LuCuS_2 and plot the results. For LuCuS_2 , the isotopic ratio of $1/T_1$ [$^{65}(1/T_1)/^{63}(1/T_1)$] is 0.88, which is close to the square of the quadrupole-moment ratio $(^{65}Q/^{63}Q)^2 \sim 0.86$. This indicates that in LuCuS_2 , $1/T_1$ is determined by the elec-

tric quadrupole relaxation originating from the phonon dynamics. The low-temperature $1/T_1$ of LuCuS_2 is quite small. In contrast, for YbCuS_2 , the isotopic ratio of $1/T_1 \sim 1.14$ coincides with the square of the gyromagnetic ratios $(^{65}\gamma/^{63}\gamma)^2 \sim 1.15$, indicating that $1/T_1$ is determined by the magnetic relaxation from the Yb^{3+} moments. $1/T_1$ exhibits a broad maximum at approximately 50 K, where the magnetic entropy reaches $R \ln 2$, as expected for the Kramers doublet ground state in specific-heat measurements. Note that $1/T_1$ gradually decreases below 50 K, which may be related to the entropy release observed in the specific-heat measurements [18]. Below 5 K, $1/T_1$ becomes constant, suggesting that the local moments fluctuate with a short-range correlation. This behavior agrees with the theoretical prediction for the one-dimensional (1-D) spin chain [26], and it has been observed in the $S = 1/2$ 1-D cuprate antiferromagnet [27, 28]. On the other hand, the absence of the critical slowing down behavior around T_0 is quite a contrast to the divergence behavior of $1/T_1$ observed in the zigzag chain compound CaV_2O_4 [29] and 1-D cuprate antiferromagnets near T_N [27, 28] where the magnetic order occurs due to interchain coupling. The absence of the slowing down behavior is likely to be related to the character of the FO phase transition [23].

Below T_0 , $1/T_1$ decreases rapidly; it is roughly proportional to T^5 down to 0.5 K. In general, $1/T_1$ of local-moment frustrated systems, such as the triangular Heisenberg antiferromagnet, is determined by the two-magnon process. It can be expressed as $1/T_1 \propto T^{2D-1}$ for $T \gg \Delta$, where Δ is the spin gap, and D ($= 3$ or 2) is the dimensionality of the spin-wave dispersion [30–33]. In YbCuS_2 , $D = 3$ is likely. Conversely, peculiar T -linear behavior was observed below 0.5 K. Theoretically, $1/T_1$ decreases exponentially [$1/T_1 \sim \exp(-\Delta/T)$] for $T \ll \Delta$ at low temperatures in conventional semiconducting antiferromagnets with a spin gap. Thus, the T -linear behavior suggests the presence of gapless excitation, which makes YbCuS_2 quite different from conventional antiferromagnets.

We note that similar T -linear behavior of $1/T_1$ below transition temperature was reported in several kagomé systems such as Zn-brochantite $\text{ZnCu}_3(\text{OH})_6\text{SO}_4$ [34] and volborthite $\text{Cu}_3\text{V}_2\text{O}_7(\text{OH})_2 \cdot 2\text{H}_2\text{O}$ [35, 36]. These compounds show the phase transition, and T -linear behavior of $1/T_1$ was observed below the transition temperature. To explain these behaviors, particle-hole excitations by spinons (fermionic elementary excitations), which are analogous to metallic excitations, were proposed [34–36] since the experimental value of $1/T_1 T$ is non-negligibly large. In fact, we also point out that the experimental value of $1/T_1 T$ in YbCuS_2 at 0.1 K ($\sim 14 \text{ s}^{-1} \text{ K}^{-1}$) is larger than that in a Cu-metal ($\sim 0.83 \text{ s}^{-1} \text{ K}^{-1}$) [37] by more than one order of magnitude.

Quite recently, novel gapless excitation has been observed in various semiconducting Kondo-lattice materials such as YbB_{12} [38] and YbIr_3Si_7 [39]. In these compounds, although the band gap opens at a low temper-

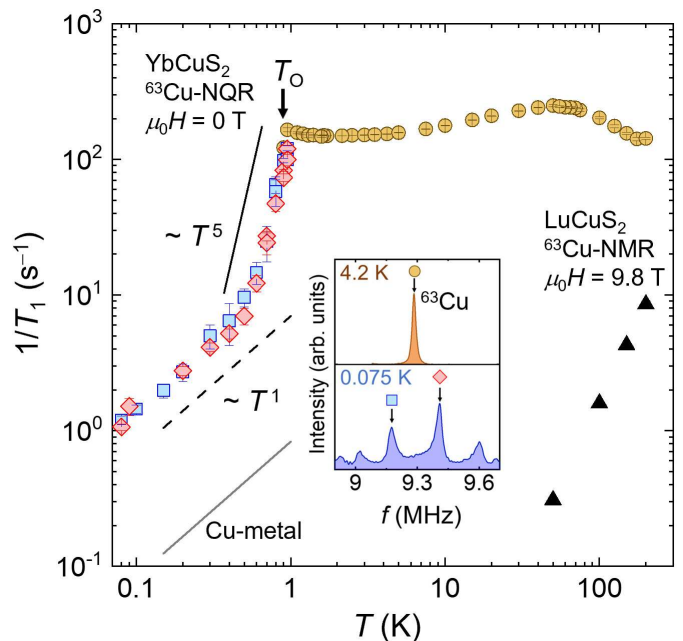


FIG. 4. (Color online) Temperature dependence of the nuclear spin-lattice relaxation rates $1/T_1$ of YbCuS_2 and a non-magnetic reference compound LuCuS_2 : the circles denote the ^{63}Cu -NQR $1/T_1$ in the PM state of YbCuS_2 . The diamonds and squares represent $1/T_1$ in the AFM state of YbCuS_2 . The black triangles indicate ^{63}Cu -NMR $1/T_1$ in LuCuS_2 for $\mu_0 H = 9.8$ T. The gray solid line denotes $1/T_1$ in a Cu-metal [37]. The inset shows the ^{63}Cu -NQR spectra measured at 4.2 K and 0.075 K. The spectrum peaks at which $1/T_1$ was measured are denoted by the symbols.

ature due to the hybridization between the localized f and the conduction electrons, quantum oscillation at high fields and the finite residual term in the specific heat and thermal conductivity experiments were observed [38, 39]. These results suggest the presence of gapless and charge-neutral excitations in the bulk properties, which are proposed to result in a quantum spin liquid with a spinon Fermi surface and the Majorana Fermi liquid. We note the possibility that the large gapless excitation observed at low temperatures in YbCuS_2 might arise from such exotic Fermi liquid states, although YbCuS_2 is a conventional semiconductor. To confirm this possibility, it is crucially important to prepare high quality single crystals for thermal conductivity and quantum oscillation measurements.

In conclusion, we performed $^{63}/^{65}\text{Cu}$ -NMR/NQR measurements on powder samples of YbCuS_2 in which the Yb ions form a zigzag chain along the orthorhombic a -axis. Below $T_0 \sim 0.95$ K, multi peaks affected by the internal magnetic fields appear; they coexist with the PM signal down to 0.85 K, indicating that the FO AFM phase transition occurs at T_0 . In addition, $1/T_1$ decreases abruptly below T_0 and exhibits T -linear behavior below 0.5 K. The significantly large $1/T_1 T$ value—more than one order of magnitude larger than the value for metallic Cu—suggests

the presence of novel gapless spin excitation originating from exotic fermions. Our finding of the large gapless excitation unveils the presence of unknown fermionic quasiparticle in frustrated magnets.

ACKNOWLEDGMENTS

The authors would like to thank Y. Maeno, S. Yonezawa, A. Ikeda, and Y. Matsuda for valuable dis-

cussions. This work was supported by the Kyoto University LTM Center, Grants-in-Aid for Scientific Research (Grant Nos. JP15H05745, JP17K14339, JP19K03726, JP16KK0106, JP19K14657, JP19H04696, JP19H00646, and JP20H00130) and Grant-in-Aid for JSPS Research Fellows (Grant No. JP20J11939) from JSPS.

-
- [1] L. Balents, *Nature* **464**, 199 (2010).
- [2] C. K. Majumdar and D. K. Ghosh, *J. Math. Phys.* **10**, 1399 (1969).
- [3] F. D. M. Haldane, *Phys. Rev. B* **25**, 4925 (1982).
- [4] K. Okunishi and T. Tonegawa, *J. Phys. Soc. Jpn.* **72**, 479 (2003).
- [5] T. Hikihara, L. Kecke, T. Momoi, and A. Furusaki, *Phys. Rev. B* **78**, 144404 (2008).
- [6] T. Hikihara, T. Momoi, A. Furusaki, and H. Kawamura, *Phys. Rev. B* **81**, 224433 (2010).
- [7] N. Maeshima, M. Hagiwara, Y. Narumi, K. Kindo, T. Kobayashi, and K. Okunishi, *J. Phys.: Condens. Matter* **15**, 3607 (2003).
- [8] M. Hase, H. Kuroe, K. Ozawa, O. Suzuki, H. Kitazawa, G. Kido, and T. Sekine, *Phys. Rev. B* **70**, 104426 (2004).
- [9] S. Furukawa, M. Sato, and S. Onoda, *Phys. Rev. Lett.* **105**, 257205 (2010).
- [10] M. Pregelj, A. Zorko, O. Zaharko, H. Nojiri, H. Berger, L. Chapon, and D. Arçon, *Nat. Commun.* **6**, 7255 (2015).
- [11] Y. Li, H. Liao, Z. Zhang, S. Li, F. Jin, L. Ling, L. Zhang, Y. Zou, L. Pi, Z. Yang, J. Wang, Z. Wu, and Q. Zhang, *Sci. Rep.* **5**, 16419 (2015).
- [12] Y. Li, G. Chen, W. Tong, L. Pi, J. Liu, Z. Yang, X. Wang, and Q. Zhang, *Phys. Rev. Lett.* **115**, 167203 (2015).
- [13] Y. Li, D. Adroja, P. K. Biswas, P. J. Baker, Q. Zhang, J. Liu, A. A. Tsirlin, P. Gegenwart, and Q. Zhang, *Phys. Rev. Lett.* **117**, 097201 (2016).
- [14] K. M. Ranjith, S. Luther, T. Reimann, B. Schmidt, P. Schlender, J. Sichelschmidt, H. Yasuoka, A. M. Strydom, Y. Skourski, J. Wosnitza, H. Kühne, T. Doert, and M. Baenitz, *Phys. Rev. B* **100**, 224417 (2019).
- [15] L. D. Gulay and I. D. Olekseyuk, *J. Alloys Compd.* **402**, 89 (2005).
- [16] T. Murugesan and J. Gopalakrishnan, *Indian J. Chem.* **22A**, 469 (1983).
- [17] Y. Ohmagari, Y. Yamane, T. Onimaru, K. Umeo, Y. Shimura, and T. Takabatake, *JPS Conf. Proc.* **30**, 011167 (2020).
- [18] Y. Ohmagari, T. Onimaru, Y. Yamane, Y. Shimura, K. Umeo, T. Takabatake, H. Sato, N. Kikugawa, T. Terashima, H. T. Hirose, and S. Uji, *J. Phys. Soc. Jpn.* **89**, 093701 (2020).
- [19] P. Blaha, K. Schwarz, F. Tran, R. Laskowski, G. K. Madsen, and L. D. Marks, *WIEN2k*, An augmented plane wave + local orbitals program for calculating crystal properties (Karlheinz Schwarz, Techn. Universität Wien, Vienna, 2018).
- [20] K. Momma and F. Izumi, *J. Appl. Crystallogr.* **44**, 1272 (2011).
- [21] When we assumed that the coupling between the nuclear Cu spin and Yb moments arises from the classical dipolar interaction, the magnitude of the hyperfine interaction is estimated as $0.07 \text{ T}/\mu_B$, resulting in $0.3 \mu_B/\text{Yb}$. This suggests that the ordered moment is much smaller than the effective moment of the CEF ground state ($1.3 \mu_B/\text{Yb}$).
- [22] M. Rotter, M. Tegel, D. Johrendt, I. Schellenberg, W. Hermes, and R. Pöttgen, *Phys. Rev. B* **78**, 020503 (2008).
- [23] S.-H. Baek, N. J. Curro, T. Klimczuk, E. D. Bauer, F. Ronning, and J. D. Thompson, *Phys. Rev. B* **79**, 052504 (2009).
- [24] D. G. Franco, Y. Prots, C. Geibel, and S. Seiro, *Phys. Rev. B* **96**, 014401 (2017).
- [25] T. Sakakibara, S. Nakamura, S. Kittaka, M. Kakihana, M. Hedo, T. Nakama, and Y. Ōnuki, *J. Phys. Soc. Jpn.* **88**, 093701 (2019).
- [26] S. Sachdev, *Phys. Rev. B* **50**, 13006 (1994).
- [27] K. Ishida, Y. Kitaoka, Y. Tokunaga, S. Matsumoto, K. Asayama, M. Azuma, Z. Hiroi, and M. Takano, *Phys. Rev. B* **53**, 2827 (1996).
- [28] M. Takigawa, N. Motoyama, H. Eisaki, and S. Uchida, *Phys. Rev. Lett.* **76**, 4612 (1996).
- [29] X. Zong, B. J. Suh, A. Niazi, J. Q. Yan, D. L. Schlagel, T. A. Lograsso, and D. C. Johnston, *Phys. Rev. B* **77**, 014412 (2008).
- [30] T. Moriya, *Prog. Theor. Phys.* **16**, 23 (1956).
- [31] T. Moriya, *Prog. Theor. Phys.* **16**, 641 (1956).
- [32] S. Maegawa, *Phys. Rev. B* **51**, 15979 (1995).
- [33] H. Takeya, K. Ishida, K. Kitagawa, Y. Ihara, K. Onuma, Y. Maeno, Y. Nambu, S. Nakatsuji, D. E. MacLaughlin, A. Koda, and R. Kadono, *Phys. Rev. B* **77**, 054429 (2008).
- [34] M. Gomilšek, M. Klanjšek, R. Zitko, M. Pregelj, F. Bert, P. Mendels, Y. Li, Q. M. Zhang, and A. Zorko, *Phys. Rev. Lett.* **119**, 137205 (2017).
- [35] M. Yoshida, M. Takigawa, H. Yoshida, Y. Okamoto, and Z. Hiroi, *Phys. Rev. Lett.* **103**, 077207 (2009).
- [36] F. Bert, D. Bono, P. Mendels, F. Ladieu, F. Duc, J.-C. Trombe, and P. Millet, *Phys. Rev. Lett.* **95**, 087203 (2005).
- [37] G. C. Carter, L. H. Bennett, and D. J. Kahan, *Metallic Shifts in NMR*, Part I (Pergamon, London, 1977).
- [38] Y. Sato, Z. Xiang, Y. Kasahara, T. Taniguchi, S. Kasahara, L. Chen, T. Asaba, C. Tinsman, H. Murayama, O. Tanaka, Y. Mizukami, T. Shibauchi, F. Iga, J. Singleton, L. Li, and Y. Matsuda, *Nat. Phys.* **15**, 954 (2019).

- [39] Y. Sato, S. Suetsugu, T. Tominaga, Y. Kasahara, S. Kasahara, T. Kobayashi, S. Kitagawa, K. Ishida, R. Peters, T. Shibauchi, A. H. Nevidomskyy, L. Qian, J. M. Moya, E. Morosan, and Y. Matsuda, arXiv:2103.13718 (2021).